UCRL- 86710
PREPRINT

Laser-Damage Thresholds of Thin-Film Optical Coatings at 248 nm

D. Milam
F. Rainer
W. H. Lowdermilk

This paper was prepared for submittal to
1981 Boulder Damage Symposium
Boulder, Colorado
November 17-18, 1981

December 11, 1981

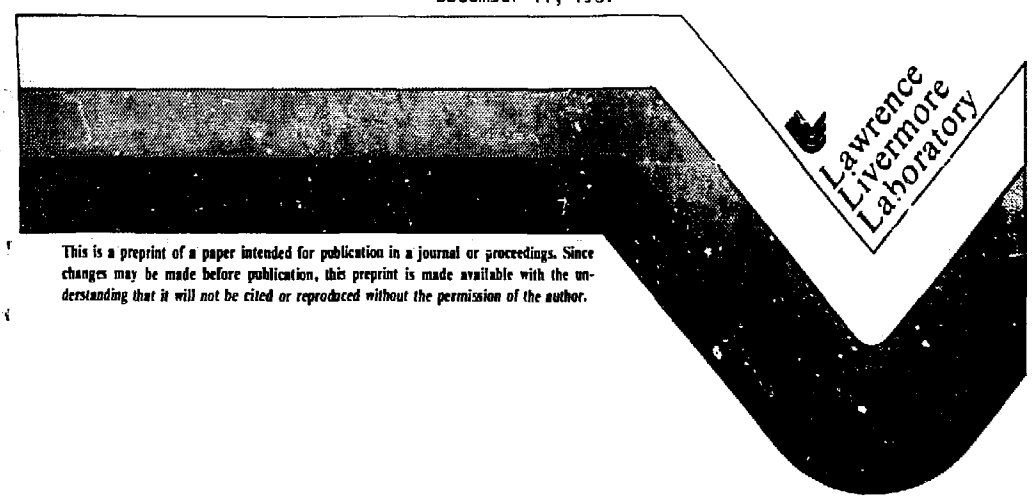

Laser Damage Thresholds of Thin Film Optical Coatings at 248 nm*

F. Rainer, D. Milam and W. H. Lowdermilk

Lawrence Livermore National Laboratory

Livermore, California 94550

UCRL--86710

DE82 007574

We have measured the laser-induced damage thresholds for 248 nm wavelength light of over 100 optical coatings from commercial vendors and research institutions. All samples were irradiated once per damage site with temporally multi-lobed, 20-ns pulses generated by a KrF laser. The survey included high, partial, and dichroic reflectors, anti-reflective coatings, and single layer films. The samples were supplied by ten vendors. The majority of samples tested were high reflectors and antireflective coatings. The highest damage thresholds were 8.5 to 9.4 J/cm^2 respectively. Although these represent extremes of what has been tested so far, several vendors have produced coatings of both types with thresholds which consistently exceed 6 J/cm^2. Repeated irradiations of some sites were made on a few samples. These yielded no degradation in threshold, but in fact some improvement in damage resistance. These same samples also exhibited no change in threshold after being retested seven months later.

*Work performed under the auspices of the U.S. Department of Energy by the Lawrence Livermore National Laboratory under Contract No. W-7405-ENG-48.

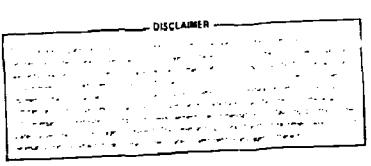

MFW

1. Introduction

Because of the interest in short wavelength lasers for inertial confinement fusion programs, we have in the past year established a facility for laser damage testing at conventional rare-gas-halide laser wavelengths. We have conducted extensive damage tests at the KrF wavelength of 248 nm with 20-ns, p-polarized pulses on high reflection (HR) and antireflection (AR) films supplied by commercial and research institutions. The test results provided a current overview of the damage resistance of commercially available samples, and established possible avenues of approach to improve damage thresholds in research grade samples. Our present goal is to achieve consistent thresholds in both HR and AR coatings exceeding 5 J/cm^2 in commercial samples.

2. Samples Tested

We began our experiments by testing representative samples of commercially available reflective and antireflective coatings purchased for use in the KrF facilities at LLNL. Most of these samples were films that were highly reflective or antireflective in normal incidence beams, but a few were AR and HR films designed for 45^0 incidence. The remainder of the samples were partial or multichroic reflectors. Except for some transparent windows with AR films on both surfaces, all samples were tested with the film as the entrance surface of the substrate. Tests on commercially available coatings were later supplemented by tests on a large number of HR, AR and single-layer films fabricated by research vendors for studies of the influence of various coating parameters on damage thresholds. The commercial and research vendors who supplied samples are listed in Table 1.

3. Experiment

3.1 Test Facility

Figure 1 shows a schematic diagram of the damage experiment. The laser consisted of a discharge-pumped KrF oscillator and amplifier with a maximum output energy of 1 J. The circularly apertured output beam passed through a set of polarizers. The first two polarizers were axially rotatable relative to the third to provide a beam which could be attenuated at will with no beam steering. The ensuing p-polarized beam was apertured to 12-mm diameter and focused by a 5-m focal length lens. The separation of the lens and sample was varied to produce at the sample surface, the largest beam with sufficient fluence to cause damage. Diagnostic beams were generated by placing a wedged splitter in the focused beam. The diagnostics included an absorbing-glass calorimeter with a 2.5-mm aperture, a multiple-exposure camera with 1-Z film for beam profiling, and a photo-diode for recording the pulse waveform. A typical temporal profile of the pulse is shown in Fig. 2. The sample, calorimeter aperture and film were all positioned in equivalent planes of the beam.

3.2 Fluence Measurements

The beam cross section at the sample surface was typically 1.5 mm in diameter, but had an irregular shape as shown in figure 2. In the smallest beams used, the most intense structure was a rectangular spike with dimensions of 150μm x 600μm (FWHM) whose peak provided uniform irradiation over an area with a diameter of 100μm. For each shot, the intensity distribution of the beam was photographically recorded at 6 to

10 incrementally decreasing exposure levels, and the pulse energy was recorded. Data for nine shots were typically recorded on each photographic plate. Computation of peak fluence from these data required a number of steps. 1) For each photographic plate, the maximum photographic densities of the multiple images recorded in one shut were measured by using a densitometer to make 20 to 50 scans across the images. The scans were laterally separated by distances ranging from 28μm to 75μm. 2) The photographic response curve (relative fluence vs. density) of each plate was generated from the set of measured densities. 3) One representative image for each of the nine shots on a plate was scanned using a 100 x 100 point array to generate an unnormalized density record of the beam energy distribution. 4) This record was numerically converted to relative fluence by use of the response curve and then normalized so that the numerical integral agreed with the pulse energy. 5) The peak of the ensuing beam profile was then read as the peak fluence for that shot.

Densitometric recordings of beam photographs usually contain isolated points of high density. In analysis of large smooth beams, such spikes are easily recognized as spurious, and do not much influence computations of fluence. In analysis of beams known to have complex shapes, it is sometimes difficult to determine whether isolated density spikes are real or spurious. Individual film grains or dust potentially influenced scans made with 28μm-square slits, and caused local density fluctuations. With larger slits, up to 57-μm square, only a few samplings were made in scans across small structures in the beam, and each density value was a spatial average of true local density values. To determine the influence of this

uncertainty, we generated, from several plates, two sets of fluence values computed by using the extremes in uncertainty in density measurements. The first used a photographic response curve based on peak measured densities; for the second we used conservatively truncated densities. When a two dimensional raster scan of a beam photograph was interpreted by use of these two response curves, beams of differing shapes were generated, and the normalized peak fluences differed. For the beam size used to generate most of the data reported here, fluences computed by using conservatively truncated densities were 9% to 20% greater than those obtained using peak measured fluences. The average difference was 14%. Therefore, density fluctuations lead to a $\pm$ 5% imprecision (range 9% to 20%), and an absolute uncertainty of about 15%.

For larger beams used to measure a few thresholds, the interpretation of density was less crucial; the mean variation in fluence values obtained from peak measured response curves versus the conservatively truncated response curves usually used was - 3%; the range was - 8% to 1%.

To test the influence of truncating the response curve at the low-density end, we constructed curves by deleting the lowest measured fluence-density datum. Fluences computed from such curves differed by less than 1% from fluences computed with nontruncated curves.

The least contribution to the composite uncertainty was that resulting from uncertainty in energy measurements. Pulse energy was measured with a Scientec absorbing-glass calorimeter which was calibrated by direct comparison with a similar LLNL absorbing-glass calorimeter calibrated to within $\pm$ 1%. The accuracy of routine measurements of KrF pulse energies ranged from 1% to 3%, depending on the magnitude of the

energy which determined the signal to noise ratio. We believe the uncertainty was typically $\pm$ 2%.

3.3 Experimental Procedure

Each sample focal area was irradiated only once and examined for damage. Damage was defined to be a permanent alteration of the sample surface that was detectable by examination of the site before and after irradiation. Comparison was done by naked eye and both visually and photographically by either bright or dark field Nomarski microscopy at magnifications ranging from 55 to 1060. In all but the most damage resistant samples the damage consisted of microscopic pits spaced by a few μm. As a set these occupied an area whose shape corresponded to a section through the fluence cross section. The micropit spacing on the best samples, about 100μm, was comparable to the width of the tip of the most intense structure in the beam.

We tested an average of seven sites on each sample. The damage threshold was defined to be the median value of the highest fluence that caused no damage and the lowest fluence that produced damage. The width of this fluence range and the uncertainties in individual fluence values were considered in assigning threshold uncertainty. For 90% of the samples, there was no mixing of damaging and nondamaging fluences that could not be attributed to fluence uncertainty. This, and the close spacing of the pits resulting from damage, indicated that we performed large-spot testing of these samples. In a few low-threshold samples, which had visually apparent large-scale variations in film quality, and in some high-threshold films with low spatial densities of damage

susceptible defects, the crossover range between damaging and nondamaging fluences greatly exceeded the uncertainty in individual fluence values. For these samples, we assigned a conservative threshold based on the lowest fluences that caused damage, since the defects responsible for damage at these lower fluences would always be encountered by a larger beam.

4. Test Results

4.1 Highly Reflective Coatings

Figure 3 shows a histogram of the measured laser damage thresholds of 77 HR coatings. The white portions represent samples from commercial vendors. These had, for the most part, already been used in LLNL laser systems so that many were several years old and already damaged. The shaded portions represent various types of research grade samples which were either sputter deposited, e-beam deposited without overcoats or e-beam deposited with overcoats. For certain parameters with the overcoated e-beam deposited samples consistently high thresholds in excess of 6 J/cm^2 were measured. The median damage thresholds and number of samples tested for each category are summarized in table 2.

Seven months after the initial tests, we retested some of these latter samples and obtained the same results within experimental error indicating no significant effects due to aging or handling (fig. 4). These tests were typically conducted with only one shot per sample area. To study the effects of multiple irradiations we retested some of these same samples putting from 3 to 14 shots on a site before moving to a new area. The fluence levels per test area ranged from 23% to 114% of the

measured single shot threshold. The small size of our beam and shot to shot variation in fluence precluded a more systematic study of the effects of multiple irradiations and sub-threshold laser hardening on damage thresholds. However, for these limited tests there was no indication that multiple irradiations produced damage at or below our measured thresholds.

4.2 Antireflective Coatings

In figure 5 we show a histogram of the damage thresholds of 43 AR films. These data are also summarized in table 2. Unlike coatings tested at 1064 nm and its harmonics, the median thresholds of both commercial AR coatings and research AR coatings without undercoats were higher than median thresholds of corresponding HR films. However, the best sets of HR research samples tested were still superior to the best sets of AR research samples. The latter coatings had damage thresholds up to 6 J/cm^2.

4.3 Single Layer Films

We measured thresholds for a few single layer films. Figure 6 shows the median thresholds of films of three materials deposited by e-beam evaporation and by sputtering. In general, the e-beam deposited films had higher thresholds than the comparable sputtered films. High reflectors made with these compositions had damage thresholds that ranked in the same order, but further tests are needed before definitive conclusions can be drawn about the correlation of thresholds for single layer and HR films.

5. Conclusions

We have measured laser damage thresholds of HR and AR films from a variety of commercial and research institutions. Our results have shown the status of currently available coatings and the degree of improvement obtainable by the variation of coating parameters. Thresholds exceeding 6 J/cm^2 at 248 nm with 20-ns pulses were observed for both HR and AR films.

6. Acknowledgements

The authors wish to express their thanks to their colleagues S. Brown, C. Dittmore, J. Goldhar, G. Murphy, J. Odegard, S. Peluso, R. Rapoport and M. Taylor. It was only with their cooperation that this facility was built and maintained and the measurements taken.

Table 1. Commercial vendors and research institutions.

Acton Research Corp.	Laser Optics
Airtron Optical & Magnetic Components	Optical Coating Laboratory, Inc.
Battelle Pacific Northwest Laboratory	Optico Glass Fabrication
CVI	Oriel
Design Optics	Spectra-Physics

Table 2. Median laser damage thresholds of thin film coatings at 248 nm, 20 ns

	HR		AR	
Type	Threshold (J/cm^2)	Number tested	Threshold (J/cm^2)	Number tested
Commercial	1.8	20	3.3	19
Research (sputter deposited)	1.0	12	--	--
Research (e-beam deposited) nonovercoated HR, nonundercoated AR	3.1	15	4.2	8
Research (e-beam deposited) overcoated HR, undercoated AR	6.3	30	5.4	16

Figure Captions

1. Schematic diagram of the KrF laser damage test facility.

2. (a) Temporal profile of the laser pulse; (b) spatial cross section of the beam at the damage plane.

3. Laser damage thresholds of 77 highly reflective coatings.

4. Threshold comparisons after 7 months; multiple irradiations of a single site.

5. Laser damage thresholds of 43 antireflective coatings.

6. Median laser damage thresholds of single layer films.

KrF LASER DAMAGE TEST FACILITY

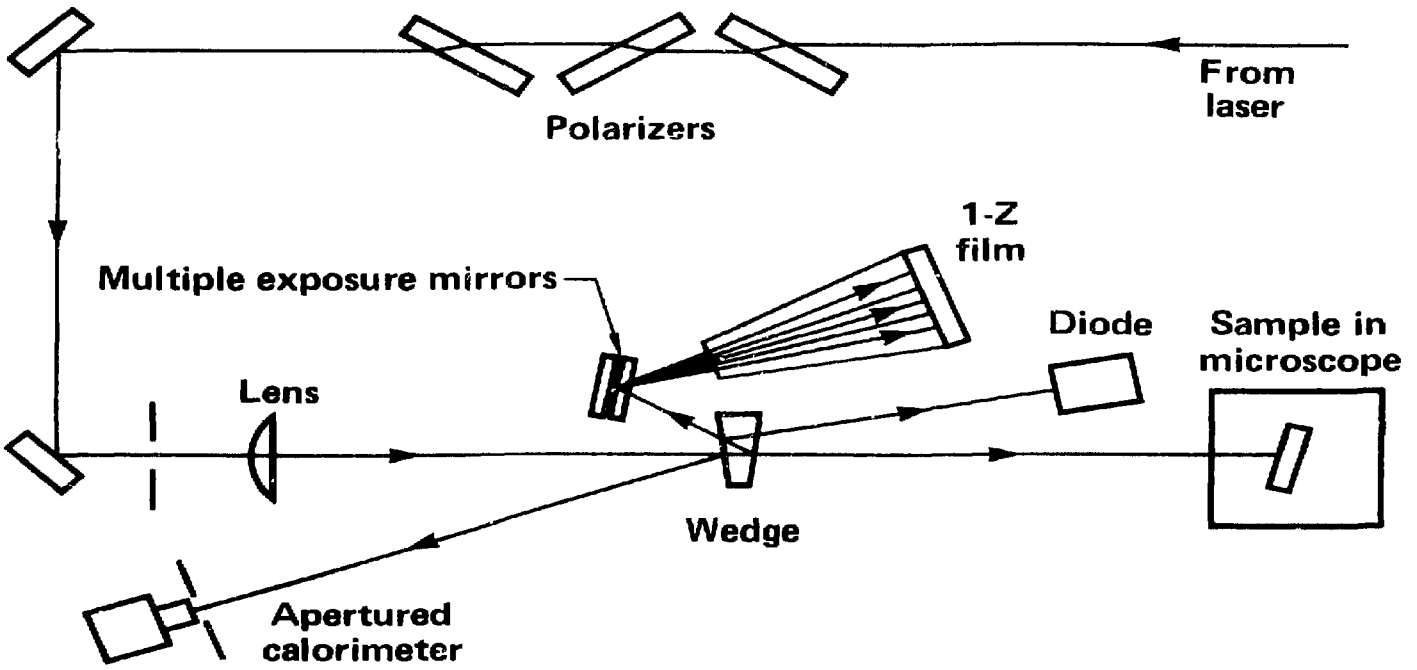

04-02-1081-3544

Figure 1

TEMPORAL AND SPATIAL PROFILES OF THE KrF BEAM

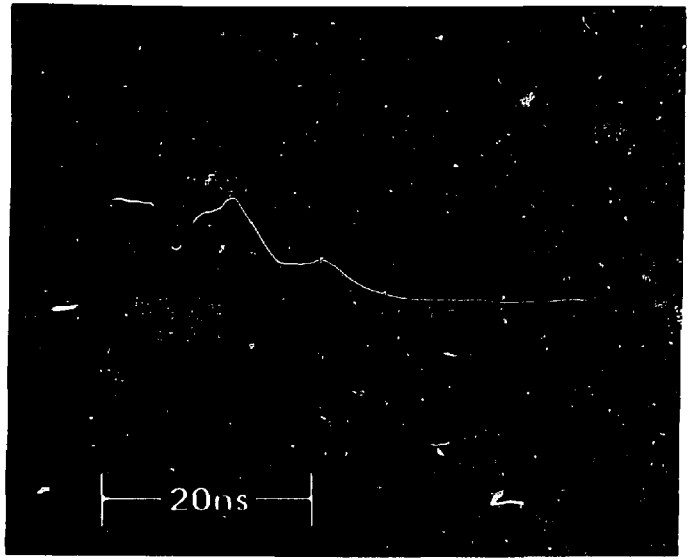

Figure 2a

Figure 2b

50-00-0181-0179

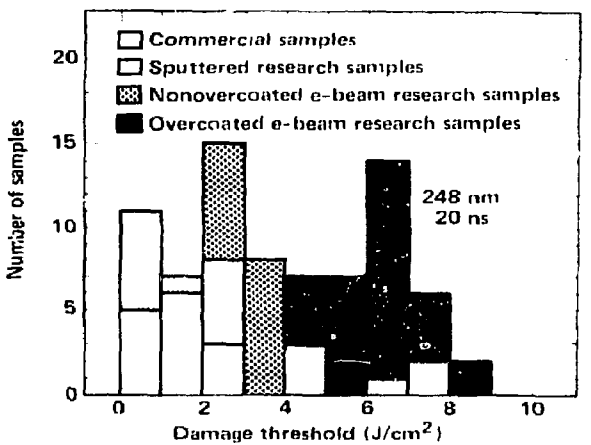
Commercial samples
Sputtered research samples
Nonovercoated e-beam research samples
Overcoated e-beam research samples
248 nm
20 ns
Number of samples
Damage threshold (J/cm²)
0
5
10
15
20
0
2
4
6
8
10

Figure 3

REPEATED TESTS (AFTER 7 MONTHS) AND MULTIPLE SHOTS PER SITE

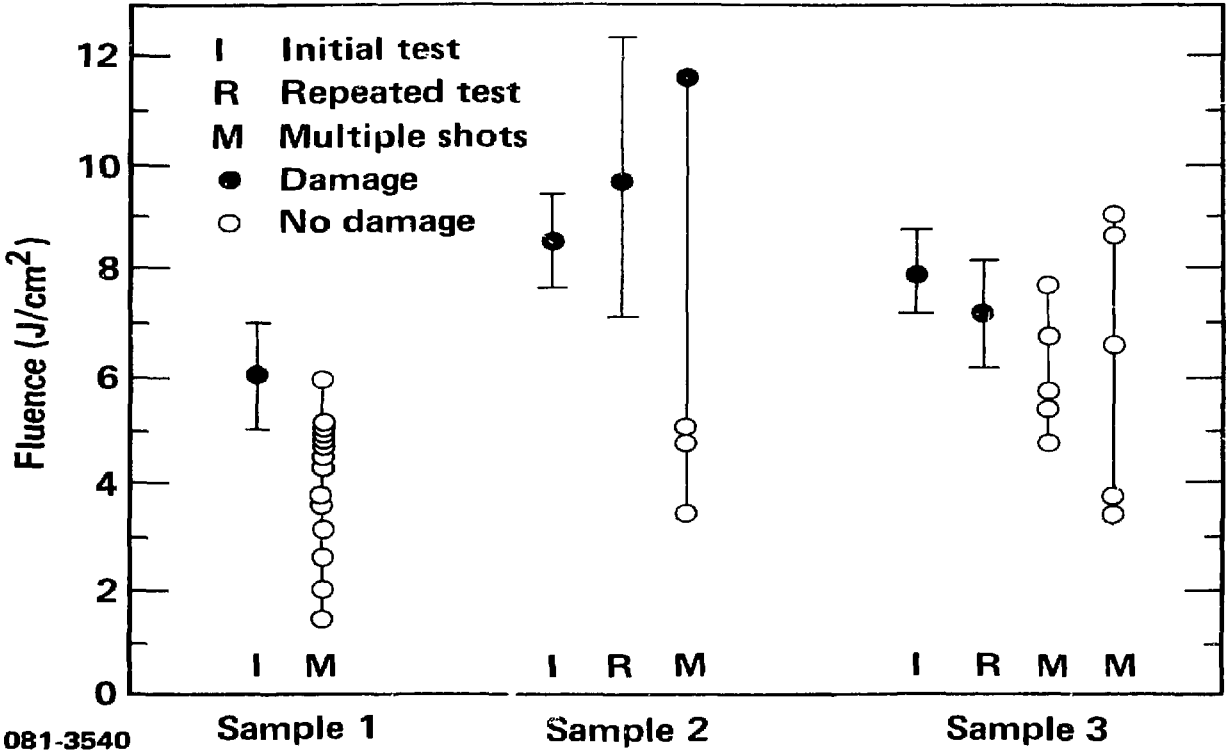

Figure 4

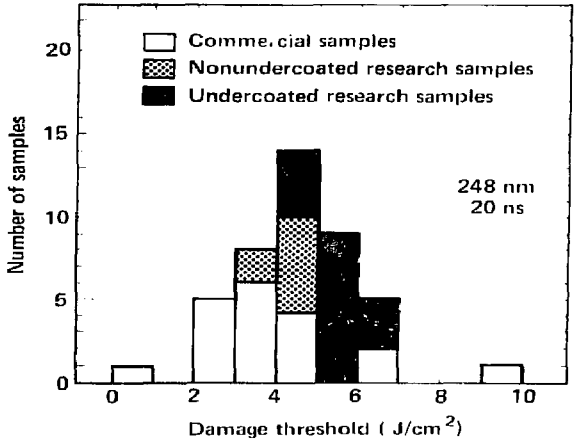
Commercial samples
Nonundercoated research samples
Undercoated research samples
248 nm
20 ns
Number of samples
Damage threshold (J/cm 2)
0
5
10
15
20
0
2
4
6
8
10

Figure 5

LASER DAMAGE THRESHOLDS OF SINGLE LAYER FILMS

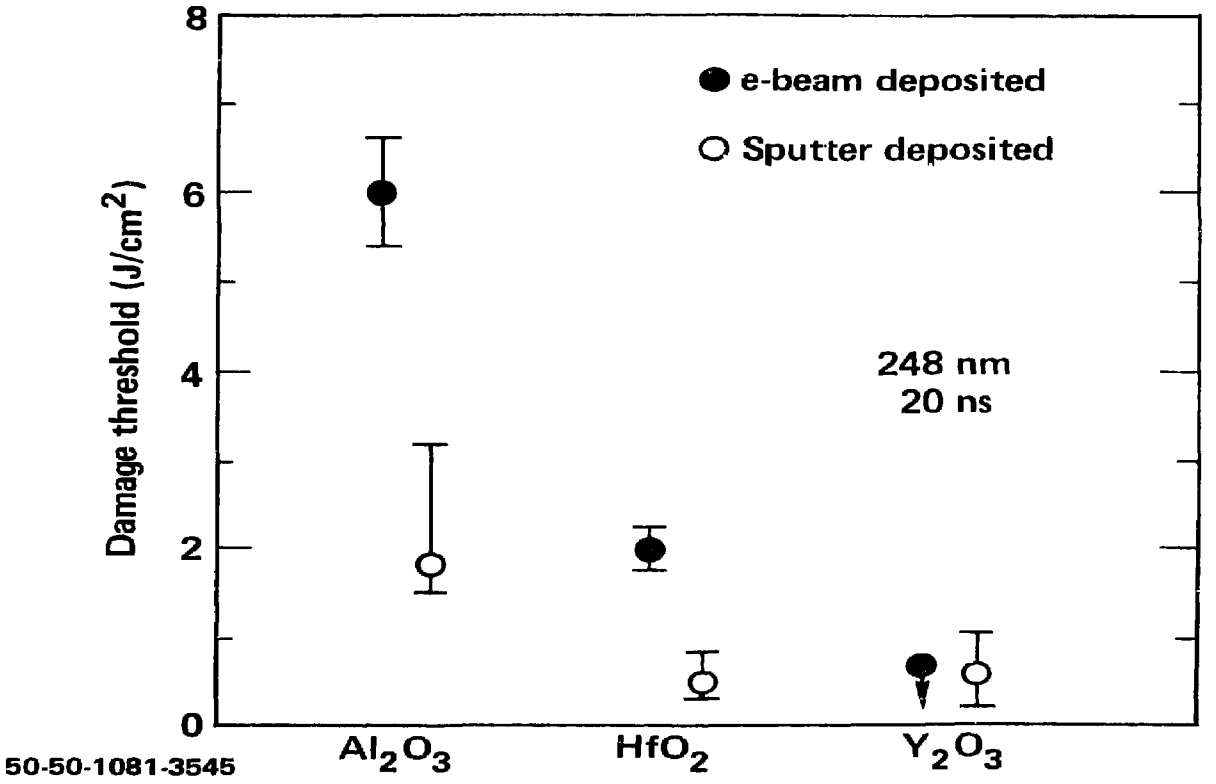

Figure 6